Cucurbit[n]uril-Immobilized Sensor Arrays for Indicator-Displacement Assays of Small Bioactive Metabolites

Chunting Zhong, Changming Hu, Ravi Kumar, Vanessa Trouillet, Frank Biedermann,* and Michael Hirtz*

ABSTRACT: The patterned immobilization of chemosensors into nano/micro arrays has often boosted utilization in diagnostics and environmental sensing applications. While this is a standard approach for biosensors, e.g., with antibodies, other proteins, and DNA, arraying is not yet adopted widely for supramolecular chemosensors which are still predominantly used in solution systems. Here we introduce the patterned immobilization of cucurbit[n]urils (CBn) into multiplexed microarrays and elucidate their prospects for the advancement of surface bound indicator displacement assays to detect small molecule analytes. The microarrays were generated by microchannel cantilever spotting of functionalized CBn and subsequent self assembly of the corresponding indicator dyes from solution.

Cucurbit[n]uril Sensor Array

Enhanced sensitivity of surface bound microarrays was established in demonstrations with small bioactive metabolites (spermine, amantadine, and cadaverine) compared to bulk assays. Furthermore, the integration of the CBn/indicator microarrays into microfluidic channels provides an efficient route for real time monitoring of the sensing process, allows easier handling, and reduces need for analyte volume. The concept was further extended to differential sensing of analytes on diplex or multiplex CBn/indicator microarrays, opening up a route for multicomponent sensing of small molecule analytes in complex liquids.

KEYWORDS: host−guest, indicator displacement assays, microarrays, microchannel cantilever spotting, chemosensors
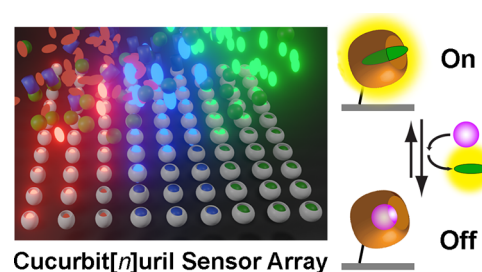
■ INTRODUCTION

The transition of molecule sensor components from bulk liquid onto solid substrates has a long history for sensing applications.[1] For biosensors such as antibodies and DNA,[2] micropatterned or nanopatterned immobilization onto the surface has been a game changer in applications ranging from research in genomics and proteomics to the detection of disease markers in diagnostics.[3] Micro and/or nanopatterning of chemosensors generates more and more potential application prospects with the transition from solution to surface bound systems showing advantages in biosensing, e.g., metals,[4] amino acids,[5] proteins,[6] and small molecule cell metabolites.[7] Micropatterned chemosensors greatly reduce the use of chemosensor materials and analytes, ease handling and readout, and allow for integration in microfluidics or devices, while enabling multiplexed detection.[8] In particular, it enables point of care or even at home testing, e.g., for glucose monitoring in diabetes[9] or for immunoassays detecting HIV, HCV, SARS CoV 2, and other viral infections.[10] The micro patterning approaches applied above include photolithography, noncontact and contact printing, and different scanning probe lithography (SPL) techniques, among which in particular microchannel cantilever spotting (μCS), which directly writes inks on surfaces, offers an attractive new route for array miniaturization and enables multiplexing (i.e., the deposition of different compounds in close vicinity within the same micropattern).[11−13]

Molecular probes and chemosensors typically engage in covalent reactions and noncovalent complex formation, respectively. In some cases, it is also possible to exploit a unique chemical reactivity of analytes directly for sensing. In general, two complementary approaches for the design of molecular sensors are most commonly adopted: (i) Molecular probes operation binds analytes covalently/by reactions,[14,15] hence providing a high binding affinity between the sensor molecule and analyte. However, they need more time for sensing due to the high activation energy barrier of bond formation.[16] (ii) Chemosensors bind their target analytes through noncovalent interactions by, e.g., electrostatic or hydrogen bonding interaction for recognition.[17] The low activation energy barrier in these systems enables fast sensing, but oftentimes the practical use of chemosensors can be limited by an insufficiently low binding affinity.[18] Ideally, molecular sensors are applied for sensing that combines a high
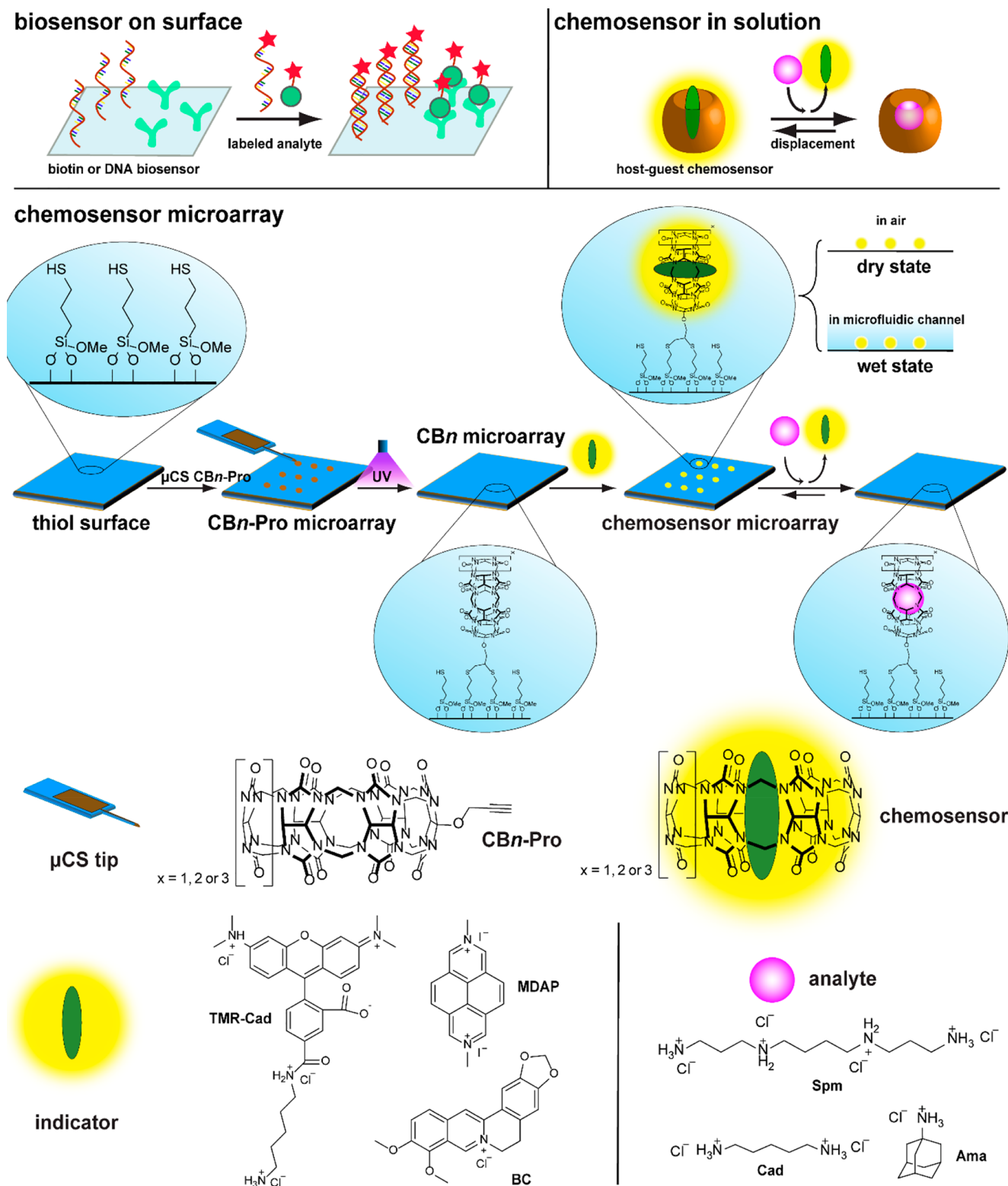
Figure 1. Comparison of two general approaches for sensing applications, biosensors on the surface and chemosensor in solution, with chemosensor microarray studied in this work.

binding strength (enabling sensitive detection of analytes) with fast response kinetics (allowing for assay operation in a practical convenient time range).

In addition to binding affinity, the analyte specificity is an important factor to consider regarding a target application. In applications such as wastewater monitoring, a chemosensor is desired to target a broad range or a whole class of compounds, e.g., organic pollutants; therefore, a rather low specificity is desirable. Conversely, for applications such as specific metabolite or hormone detection in a complex biological
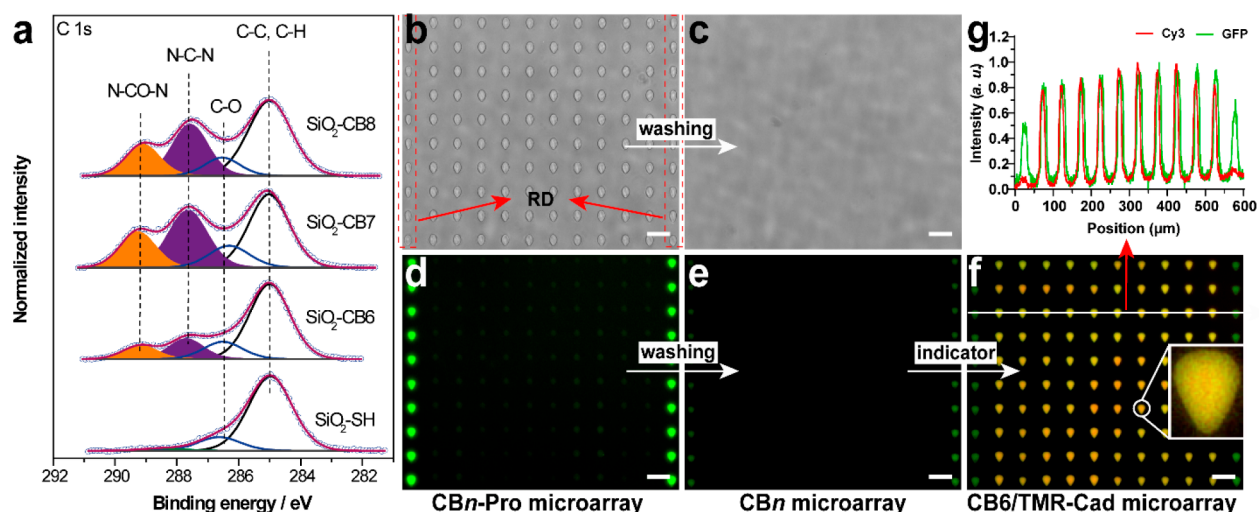
Figure 2. XPS measurement, CB*n* microarray patterning, and indicator loading. (a) C 1s XP spectra of SiO$_2$−SH, SiO$_2$−CB6, SiO$_2$−CB7, and SiO$_2$−CB8. All spectra are normalized to the maximum intensity. The two peaks at 287.6 and 289.2 eV indicate the presence of CB*n* on the surface. (b) Freshly printed CB*n* Pro microarray in bright field (BF); BDP 630/650 alkyne as a reference dye (abbreviated as RD) was marked out in a red box. (c) Immobilized CB*n* microarray in BF. Overlay of fluorescence images from Cy3 and GFP channels: (d) CB*n* Pro drop microarray after printing, (e) CB*n* microarray after UV, washing, and drying, and (f) CB6 microarray after loading with TRM Cad indicator. The inset shows the homogeneous property of microarray dots. (g) Fluorescence intensity plots along the white line in (f). Scale bars equal to 50 μm in all images. After printing, the spotted ink droplets of the 12 × 10 microarray are visible in BF. In fluorescence, only the flanking columns spotted with RD are visible. After the excess ink is washed, no observable features remain in BF, and only the RD columns appear bright in fluorescence. After incubation with TMR Cad, the CB6 section becomes visible in fluorescence.

fluid such as blood (containing many interfering molecules of similar chemical structure), a high specificity needs to be reached.

One particular promising category of supramolecular sensors is the host−guest chemosensors, which combine high binding affinity with a tunable selectivity, e.g., through size matching and exploitation of secondary noncovalent interactions.[19,20] Among the known macrocyclic hosts, glycoluril based cucurbit[*n*]urils (CB*n*) achieve record high affinities in aqueous media[21] while retaining nearly diffusion limited complexation rates for analyte binding[22] and can target many biologically,[23] medicinally,[24] and environmentally relevant analytes.[21,25−27] Unlike antibodies and protein based receptors, CB*n* based chemosensing materials can be prepared at extremely low costs and are thermally and chemically robust and thus may find future use in home and point of care applications. Harnessing the noncovalent nature of analyte/chemosensor binding, these supramolecular host−guest systems are especially used in indicator displacement assays (IDA)[28] that combine the host−guest supramolecular interaction and fluorescence signaling in one system for sensing.[24,27,29,30] Here, displacement of an environment responsive indicator dye from a host/receptor by the analyte is accompanied by readily measurable changes in the emission properties (e.g., intensity or wavelength).

To date, CB*n* based sensing assays are almost exclusively limited to solution based assays which may be one of the reasons why these systems are still rarely used for environmental monitoring or molecular diagnostics in real life settings outside of lab demonstrations. We believe that the establishment of immobilized CB*n* based chemosensors will lead to a leap forward in their "real world" applicability. Possible immobilization strategies of CB*n*/indicator chemosensors on the surface[31,32] vary from covalent linking CB*n* derivatives,[33−36] electrostatic adsorption, or UV irradiated attachment on gold[37,38] to guest mediated immobilization via

noncovalent host−guest chemistry.[39,40] While a few of them reported CB*n*/indicator chemosensors on the surface[35,36] and a patterning approach (microcontact printing) is stated for potential application,[34,36,40−42] more flexible micropatterning strategies are needed to obtain diverse CB*n*/indicator micro arrays.

Here we implemented a flexible and multiplexed micro patterning approach of CB*n*/indicator chemosensors on the surface. Functionalized CB*n*, propargyl curcubit[*n*]urils (CB*n* Pro), were micropatterned on thiol surfaces (SiO$_2$−SH) via μCS to obtain CB*n* microarrays through thiol−yne photo reaction and then activated with corresponding indicators (Figure 1). Their excellent sensing properties for IDA are evaluated with spermine (Spm, one of the key biomarkers for early stage cancer diagnosis,[43] which plays an important role in cell growth and differentiation),[44] cadaverine (Cad, one of food freshness indicators),[45] and amantadine (Ama, a medication used to treat dyskinesia associated with parkinsonism)[46] (structures shown in Figure 1).

The CB*n*/indicator microarrays are integrated into micro fluidic channels to demonstrate real time monitoring of the whole sensing process at the liquid−solid interface. Conceptually, it should be noted that the immobilization of the CB*n* into microarrays enables one to carry out the detection either in the "dry state" (after incubation with an analyte, the liquid is removed, and the sensor chip is dried in air and then imaged by fluorescence microscopy) or in the "wet state" (imaging is performed with fluid remaining on the sensor chip, e.g., when it is integrated into a microfluidic device—not to be confused with in solution IDA—as in our case the CB*n* still remain strictly coupled to the surface and do not distribute into the analyte solution); see Figure 1. The dry state enables in particular the assessment of even faint signals, as it omits optical effects, light scattering, and light absorption by the fluid, while the wet state measurements are ideal for real time monitoring of the sensing process as in the microfluidic chips,

with CBn retained and unaffected by washing steps or replacement of the analyte solution, minimizing the amount of needed materials as compared to classic in solution IDA. Thus, the immobilization allows for the additional freedom of setup tailored to application needs in comparison to traditional bulk assays. Furthermore, multiplexed CBn/indicator micro arrays that contain different CBn and even different indicators in one microarray were prepared to distinguish different analytes. These demonstrations open up a way to design micro/nanoscale chemosensor arrays and even multiplexed arrays that enable the detection of more than one analyte orthogonally.

■ RESULTS AND DISCUSSION

Surface Functionalization. As a first step, the general surface functionalization for SiO_2–SH and CBn immobilized surfaces (SiO_2–CBn) was confirmed on homogeneously coated samples by contact angle measurements and X ray photoelectron spectroscopy (XPS). SiO_2–SH surfaces were prepared on glass substrates with (3 mercaptopropyl) trimethoxysilane (MPTMS).[47] The increased contact angle of SiO_2–SH surfaces and the appearance of an S 2p doublet with S $2p_{3/2}$ at 163.5 eV (Figure S2) attributed to S–H bonds prove the successful thiol modification of the substrate. Oxidation of some of the thiol functionalities can be observed with the presence of a further doublet of weak intensity at 168.0 eV. Afterward, SiO_2–SH surfaces were homogeneously functionalized with CBn through thiol–yne photoreaction[47] to obtain SiO_2–CBn surfaces (n = 6, 7, or 8). Again, the decreased contact angles for SiO_2–CBn surfaces compared to SiO_2–SH surfaces are indicative of CBn immobilization.[48] A more direct evidence for the successful attachment of the various CBn is given by the presence of two additional components in the C 1s XPS spectra, namely, N–C–N at 287.6 eV and N–CO–N at 289.2 eV, with an expected ratio of the intensity of 2:1 (Figure 2a).

Furthermore, the corresponding N 1s peak of carbamide at 400.3 eV is detected to have a ratio of ∼1.0 to the corresponding carbon components at 287.6 eV and ∼1.5 to those at 289.2 eV, confirming the integrity of the CBn (Table S2). The relative densities of CBn to the thiol group are about 0.2 (CB6), 0.5 (CB7), and 0.5 (CB8) (Table S3), indicating the similar grafting density for CB7 and CB8 (Table S3). The purities of CBn Pro used were around 22.5% (CB6 Pro), 79.3% (CB7 Pro), and 22.4% (CB8 Pro). The lower grafting density of the CB6 surface could seem to be caused by impurities in CB6, but the CB8 surface is not affected even with the similar low purity of CB8 Pro, compared to the highly pure CB7 Pro. A more detailed discussion about the effect of the impurities is given in the section "Influence of Impurities in CBn Pro" below. Overall, these results prove the successful preparation of SiO_2–SH surfaces and subsequent immobilization of CBn by thiol–yne photoreaction.

Chemosensors Micropatterning. Having confirmed the successful immobilization of the compounds in homogeneous coatings, the next step is to create micropatterns of the immobilized chemosensor. For this, microchannel cantilevers were loaded with inks containing CBn Pro or a reference dye (abbreviated as RD, BDP 630/650 alkyne was used as a RD to mark the microarray position) and installed in the SPL system. By bringing the cantilever into contact with the desired positions on the surface for defined dwell times, the ink was allowed to flow from the cantilever reservoir to the surface by capillary forces and form the microarray spots. The process is automated to spot arrays of that desired, as visualized in Video S1. Optical micrographs (bright field) of typical microarrays after spotting are shown in Figure 2b. Here, the CBn Pro microarray and two flanking RD columns are visible before washing. The automated μCS process controls the dot size within a narrow distribution, the average feature dot radius being (8.43 ± 0.49) μm (Figure S3d, all radius distributions of the rest of the microarrays below are shown in the Supporting Information). After spotting, the patterned microarrays were placed under UV light for 10 min to facilitate the covalent binding of the CBn and the RD to the surface via thiol–yne photoreaction.[49] Then, excess ink was washed away, and no observable feature remains in the bright field (Figure 2c). In fluorescence microscopy, only the features containing the RD (first and last column) are visible (Figure 2d and e) as the CBn Pro is nonfluorescent. The CBn microarray becomes only observable in fluorescence after loading of indicator dye. For different CBn, suitable indicator dyes were chosen depending on their affinity and photophysical parameters. For CB6, tetramethylrhodamine cadaverine (TMR Cad) is a high affinity indicator dye (the tetramethylrhodamine part serves as a chromophore, while the cadaverine acts as a binding group to the CB6).[50] Due to its relatively broad emission and high intensity, it is visible in Cy3 and GFP filters (overlaid channels shown in Figure 2f, single filter channels are given in Figure S3). A normalized intensity line plot along 12 dots is shown in Figure 2g. Berberine (BC) and N,N' dimethyl 2,7,diazapyre nium (MDAP) are good indicators for CB7[51,52] and observable in GFP (Figure S3j) and DAPI (Figure S3o) channels, respectively. The above results demonstrate the establishment of surface bound CBn chemosensor microarrays visible in fluorescence, validating the proposed immobilization strategy.

Influence of Impurities in CBn-Pro. As mentioned when discussing the XPS results on homogeneous immobilization, the CBn Pro used in this work are crude products containing some percentage of pristine CBn together with their hydroxylated derivatives (CBn–OH) from reactions. While it is possible to purify these materials through repeated chromatographic separations (see the Supporting Informa tion),[34] we were interested in assessing if the crude materials that were prepared at much lower cost and effort can be as effective as the purified CBn Pro. Thus, the influence of impurities of CBn and CBn–OH to the thiol–yne photo reaction between the CBn Pro and surface thiol groups was evaluated by printed pure CB7, CB7 OH, and purified CB7 Pro (with only minor remains of CB7) microarrays (Figure S4). After UV irradiation for 10 min and washing, three microarrays were incubated with BC solution. From the fluorescence images, chemosensor microarray was found only in the CB7 Pro printed sample while no signals were detected in CB7 and CB7 OH printed samples (Figure S4a and b). Therefore, the remaining CBn and CBn–OH will not affect the CBn Pro immobilization. The printing and subsequent washing of the chemosensor arrays are also a purification process, as only the desired CBn Pro can bind covalently to the surface, thus allowing the omission of tedious chromatographic purification steps for CBn Pro.

Mono-CBn/Indicator Microarray. To demonstrate the functionality of these microarrays as IDA chemosensors, different CBn/indicator chemosensor arrays were incubated with nonchromophoric analytes. First, the performance of a
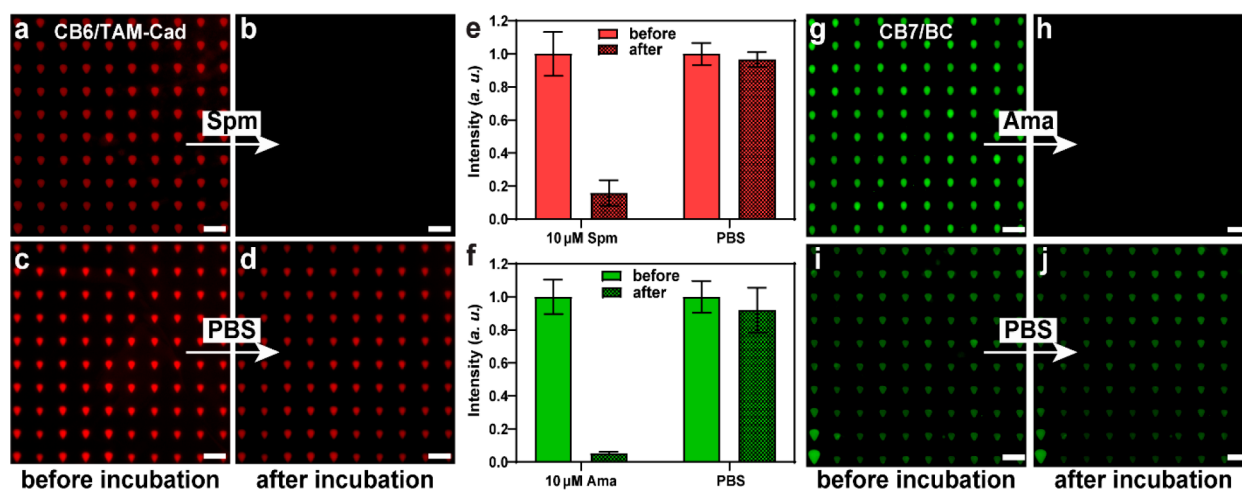
Figure 3. Mono CB*n*/indicator chemosensor microarrays. Fluorescence images of a CB6/TMR Cad microarray (a) before and (b) after incubation with 10 μM Spm; a distinct loss of fluorescence indicates analyte detection. Another CB6/TMR Cad microarray (c) before and (d) after pure PBS (1×) as a negative control, showing a smaller loss of fluorescence. Images were taken in the dry state with a 40 ms exposure time. (e) Quantification of the fluorescence intensities of CB6/TMR Cad chemosensor microarrays for Spm detection. Besides, Ama was detected on a CB7/BC microarray with corresponding fluorescence intensities shown in (f) and fluorescence images (g)−(j). Images were taken in the dry state with a 6 s exposure time. Scale bars equal 50 μm. The experimentally significant differences were evaluated using analysis of variance (ANOVA). The statistical significance was defined as $p < 0.05$.
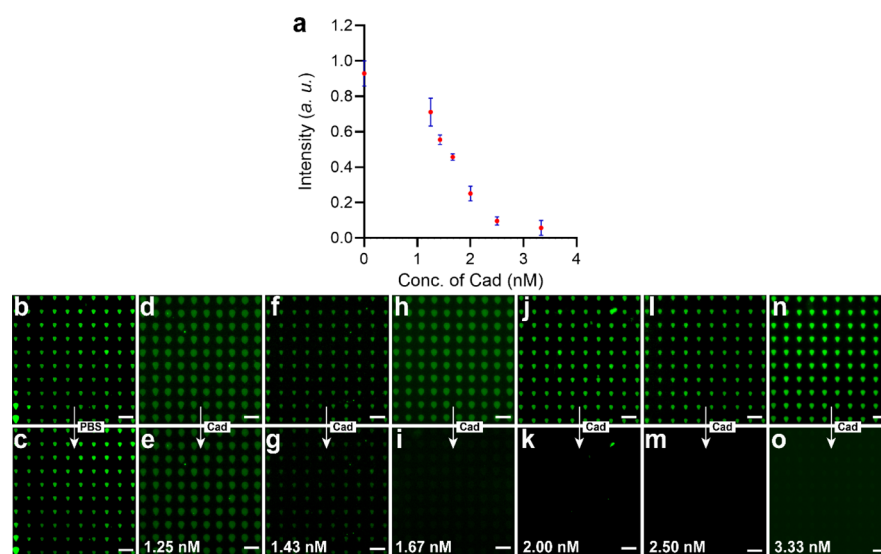

Figure 4. CB7/BC chemosensor microarray for Cad detection at a nanomolar concentration. (a) Intensity changes in different concentrations. Images of microarray for PBS control (b) and (c). Images of microarrays for Cad detection from 1.25 to 3.33 nM (d)−(o). At 1−2 nM, no full replacement is achieved.

CB6/TMR Cad microarray for detecting Spm was trialed (Figure 3, reference dye columns are cut out for easier visual comparison in all following images).

When incubation takes place with a solution of Spm in PBS, the fluorescence signal on the CB6 microarray disappears (Figure 3a and b, figures taken in the dry state, the same below if not in microfluidic channels), as the Spm replaces the indicator dye because of the higher binding affinity of CB6/Spm (log K_a = 9.52 in 50 mM sodium chloride buffer) compared to CB6/Cad (log K_a = 8.18).[50] However, the fluorescence of the microarray keeps almost constant after incubation with only PBS as a negative control for 10 min (Figure 3c and d). Quantification of the fluorescence intensity showed an obvious decrease in exposure to Spm and a small loss in the control sample (Figure 3e and Table S4). The CB7/

BC microarray was evaluated for the detection of Ama (Figure 3f−j and Table S5). The detection happened almost instantly and finished in less than 1 min. The fluorescence is absent after Ama incubation (Figure 3g and h), while fluorescent patterns remain bright after PBS incubation for 1 min (control) (Figure 3i and j). Figure 3f shows an obvious intensity decrease after Ama incubation and a small decrease in the control. Cad was detected on the CB7/BC microarray at the nanomolar level: Figure 4 shows the persisting fluorescence pattern in the control (Figure 4b and c) and faster disappearance in increasing concentrations of Cad (Figure 4d−o). The control shows a slight intensity decrease and increasing losses according to the increasing concentrations, and an incomplete replacement is achieved near from 1 to 2 nM (Figure 4a). However, in a solution based assay, more than 3 orders of
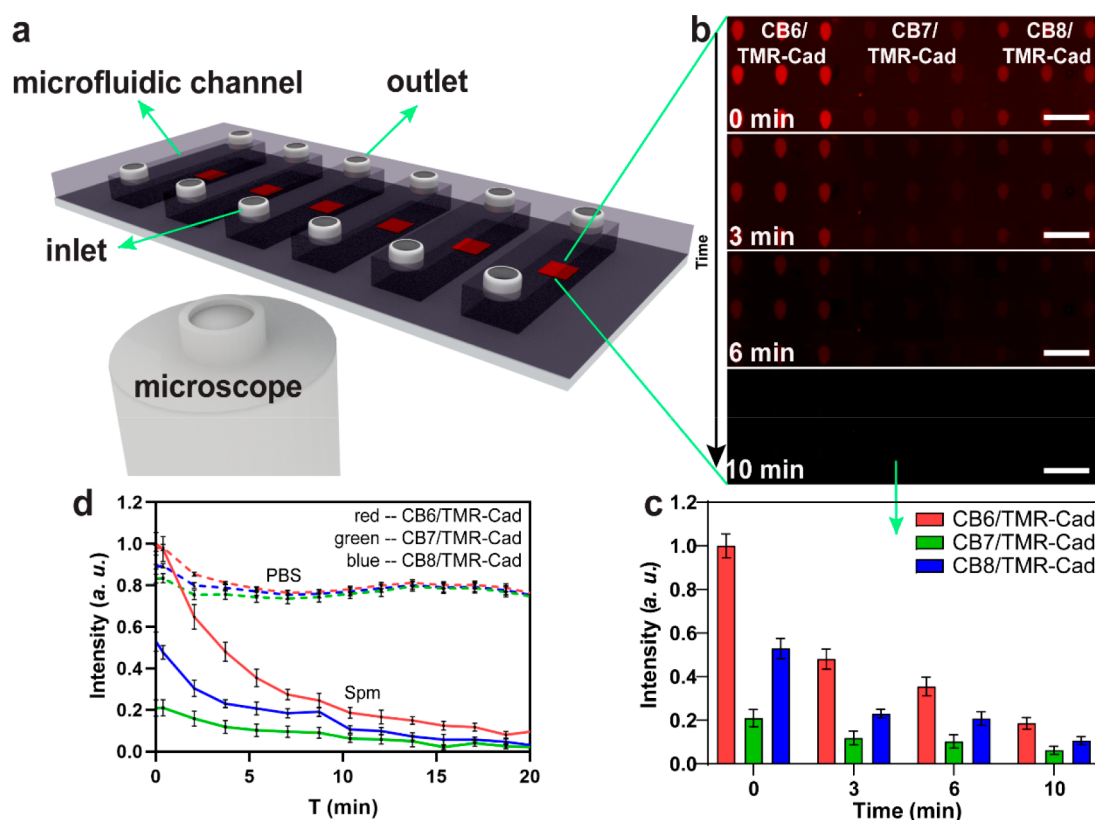
Figure 5. CB6 CB7 CB8/TMR Cad microarray for Spm detection in microfluidic channels. (a) Scheme of the microfluidic channel chip. (b) Images of chemosensor microarray containing 9 × 10 spot subpatterns of CB6, CB7, and CB8, all loaded with TMR Cad in fluorescence, at time points of 0, 3, 6, and 10 min upon incubation with 10 μM Spm. Scale bars equal to 50 μm. (c) Intensities of CB6 CB7 CB8/TMR Cad microarray at 0, 3, 6, and 10 min incubated with 10 μM Spm in PBS screenshot from live videos. (d) Graph of the fluorescence intensity time evolution of an array in PBS (negative control) and 10 μM Spm. While both samples (control and Spm) show a decrease in fluorescence intensity over time, the decrease is faster and more pronounced in the Spm case.

magnitude higher analyte concentrations (micromolar) are required to detect cadaverine through IDA, even when only low salt "minimal" buffers are used.[53] The high sensitivity of CB7/BC for Cad detection may be caused by the high ratio of analyte molecule to the available surface bound CB7 (log K_a = 8.37 in water).[54] The ratio of analyte molecules to available surface bound CBn molecules is 1.0×10^7 already for just 20 μL of analyte solution at 2.0 nM on a 10 × 10 CBn feature sensing array (calculation given in the Supporting Information). This vast excess of analyte molecules can easily and quickly replace all available indicator dye molecules in the surface bound CBn. Another effect enhancing the detection effectively (compared to in solution IDA) is that, even though the indicator dyes stay fluorescent after leaving the CBn hosts, they will diffuse away from the surface. This is at the same time the focal plane for the fluorescence detection; hence, they also do not enhance significantly the overall fluorescent background as they would in in solution IDA. However, the incomplete replacement of BC may reveal the limitation of the mass transport in liquid—solid interfaces (discussion below in the section "Equilibrium of the CBn/Indicator Microarray"). To further monitor the dynamics of the process and demonstrate the possibility of the incorporation of such microarrays into a microfluidic detection system, a microfluidic channel was mounted to a matching microscopic glass slide with CBn microarrays (Figure 5a and Figure S8). The real time monitored Cad detection shows transient replacement (Video S2). Because of the stronger binding affinity between

CB7 and MDAP (log K_a = 9.43),[54] another indicator for CB7, the replacement takes longer than that for CB7/BC. After 5 min Ama incubation, the fluorescence diminishes (Figure S9 and Table S7). The discussed results demonstrate the feasibility of mono CBn/indicator microarrays, exemplified with CB6/TMR Cad for Spm detection and CB7/BC or CB7/MDAP for Ama and Cad detection.

Regeneration of CBn Microarrays. Due to the non-covalent host—guest interaction, it is possible to regenerate CBn/indicator microarrays. Even though reuse of chemo sensors is often not desired to avoid cross contamination (e.g., in medical applications), it is nevertheless an additional corroboration for the IDA mechanism in the presented microarrays. For demonstration, a CB7/BC microarray was incubated with Cad resulting in an obvious fluorescence loss (Figure S10). For the second round, the same microarray was incubated with 100 μM BC solution to obtain the reloading of BC. The recycled CB7/BC microarray showed a reduced BC signal but was still bright enough for another feasible Cad detection. This result indicates from another perspective the mechanism of indicator replacement due to the high ratio of BC to Cad molecules on such a CB7 microarray (5.0×10^{11}, calculation given in the Supporting Information).

Di-CBn/Monoindicator Microarrays. Mono CBn/indicator microarrays have—as demonstrated above—favorable properties regarding sensitivity and will rapidly detect high affinity analytes. However, distinguishing different analytes will require specific CBn/indicator pairs, and a multiplexed
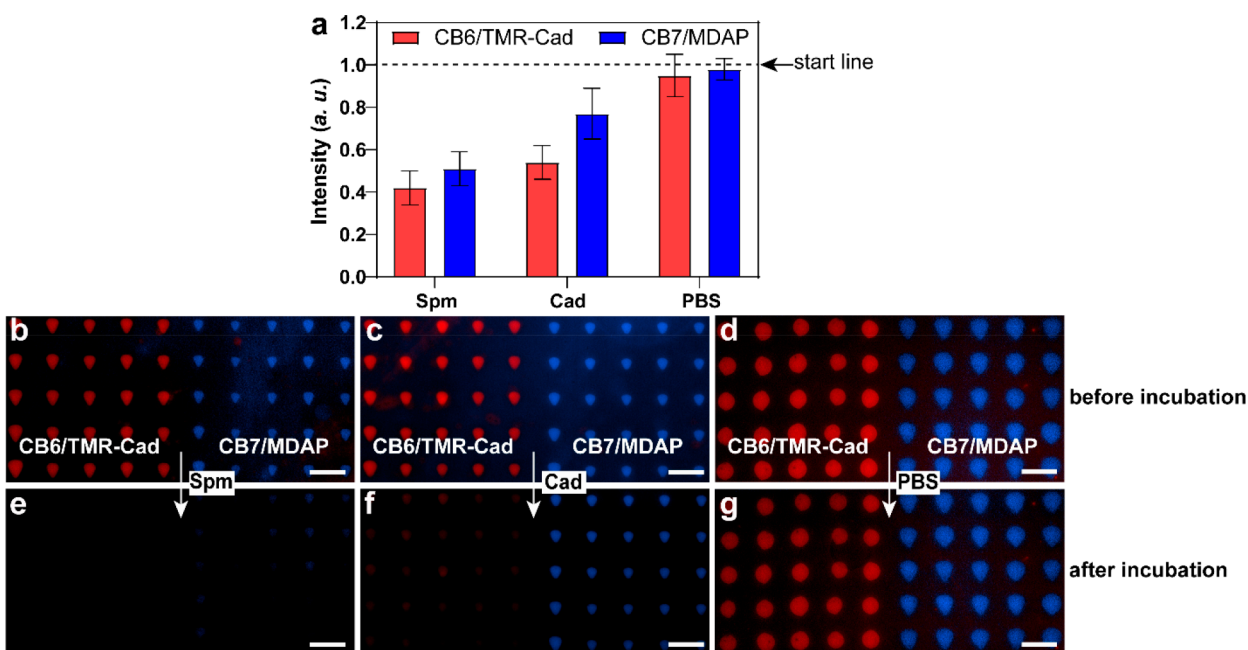
Figure 6. CB6/TMR Cad and CB7/MDAP multiplexed microarray for Cad and Spm detection. (a) Fluorescence intensity graph of Spm, Cad, and PBS control after 5 min incubation. Overlay images of three CB6/TMR Cad and CB7/MDAP multiplex microarrays (b), (c), and (d) of Cy3 (red) and DAPI channel (blue). Overlay images of these microarrays after (e) 1 μM Spm, (f) Cad, or (g) PBS incubation. Scale bars equal 50 μm. On visual inspection, both CB6/TMR Cad and CB7/MDAP sections of the microarray lose fluorescence after the Spm incubation and lose less fluorescence after Cad incubation but keep almost all fluorescence in the control.

chemosensor microarray would be much more desirable to address such limitations. One feasible approach is spotting different CBn Pro homologues within one microarray to get diplex or even multiplex microarrays with different indicator/CBn pairs. In such a scenario, indicators would be replaced by corresponding analytes, allowing sensing of different analytes on the same microarray. Toward the realization of this concept, diplex CB6 and CB7 microarrays were prepared and then incubated with respective matching indicators. BC can only assemble with CB7 as the size of BC is too large to get into the CB6 host (Figure S11 and Table S9), thus effectively controlling the molecular self assembly. After incubation with 0.1 μM Cad, fluorescence diminishes compared with the control. The same behavior is observed for MDAP, which also only assembles into the CB7 host (Figure S12 and Table S10). This duplex chemosensor was then used to detect Ama. After Ama incubation for 5 min, the fluorescence intensity diminishes again.

Multi-CBn/Monoindicator Microarray. To create a more complex multiplex microarray, CB8 Pro was spotted in addition to the CB6 Pro and CB7 Pro. Then, the prepared CB6 CB7 CB8 microarray was mounted with a microfluidic channel (Figure S8) to demonstrate real time monitoring during the whole sensing process. Here, TMR Cad can assemble into all CB hosts but in different quantities, as distinguished by brightness variation, with the fluorescence intensity of CB6 > CB8 > CB7 (Figure 5 and Table S11). The process of analyte sensing was recorded in real time after indicator loading (Video S3). The chemosensor microarrays were either incubated with PBS (as negative control) or 10 μM Spm in PBS. In both, the overall fluorescence intensity decreases over time indicating that indicator dye molecules are statistically detaching from the host and are lost out of the microarray by diffusing away, even in the case of PBS (Figure

5d). However, a clear and highly significant difference is visible, as the speed of the fluorescence intensity decrease for the Spm incubated microarray is faster and the overall decrease is significantly higher compared to the control (near complete loss of fluorescence compared to 20% decrease in the control). Furthermore, the intensity of the CB6/TMR Cad submicroarray decreases fastest upon incubation with Spm, slower for the CB8/TMR Cad, and slowest for the CB7/TMR Cad. Still (due to the different starting intensities), the obvious fluorescence intensity on visual inspection of the micrographs disappears first for the CB7 sensor (after 3 min, Figure 5b and c and Table S11), then for the CB8/TMR Cad (after 6 min), and finally for the CB6/TMR Cad sensor (after 10 min). After 10 min, the intensity is almost stable for all submicroarrays.

Di-CBn/Di-indicator Microarray. Having different affinities to different CBn, indicators visible in different fluorescence channels enable the design of multiplexed microarrays with multicolor indicators for even more complex sensing applications. To demonstrate this concept, a CB6/CB7 microarray was loaded with two indicators, TMR Cad and MDAP. This could even be done concurrently by incubating the microarray in a mixed solution with 50 μM of TMR Cad and MDAP. The two indicators self assembled into the respective surface bound CBn (Video S4). CB7 catches more MDAP due to the higher affinity while the TMR Cad assembles into the CB6. Both indicators could be directly distinguished in different fluorescence channels, with red for CB6/TMR Cad (Cy3 channel) and blue for CB7/MDAP (DAPI channel) (Figure 6, images in single channel shown in Figures S14, S15, and S16).

When such prepared microarrays are incubated with a solution of 1 μM Spm, both CB6/TMR Cad and CB7/MDAP sections of the microarray lose fluorescence due to the higher binding affinity of Spm with CB6 and CB7. In contrast, when 1

μM Cad (which is expected to bind to the CB6 host first due to the higher affinity) solution is incubated, a sharp decrease of the fluorescent signal is exclusively observed for the CB6/ TMR Cad part, while the fluorescence of the CB7/MDAP part decreases less. This shows that Cad efficiently replaced the TMR Cad in the CB6, while the MDAP in the CB7 parts remained less disturbed in the host. For the negative control, a microarray was incubated with PBS, and both parts show only a small decrease in fluorescence by the random detachment of the dye. This duplex sensing demonstrates the potential for distinguishing different analytes by replacement in submicroarray sections, even for analytes where CBn are not fully selective (as here Cad and Spm). By the addition of additional CBn components, this concept could be further expanded, eventually allowing for analyte identification by a differential response of the different submicroarray due to the size and affinity of the local host/guest system. A multiplexed CB6/ CB7/CB8 microarray was incubated with TMR Cad and MDAP mixed solution, and the CB6/CB7 sections showed predominantly the TMR Cad and the MDAP fluorescence signal, respectively, as before. Adding the GFP channel into the overlay allows even for distinguishing between the TMR Cad signal in CB6 and CB8, as for the differential shift in the spectrum of the indicator dye in the different hosts (Figure S17).

Equilibrium of the CBn/Indicator Microarray. Normally, host−guest supramolecular systems dissociate upon dilution, and the kinetics of guest dissociation is on the order of ∼1 s, so the system should quickly equilibrate upon dilution,[52,55] especially when only a monolayer of molecules patterned in the surface bound microarray is exposed to 20 μL of the buffer.[56] However, the persistence of fluorescence in the microarrays during PBS incubation shows that the indicators did not dissociate this quickly from surface immobilized CBn. The reason for this interesting phenomenon may be the increased binding affinity or equilibrium constant of the dye to the host at the interfaces, where the dielectric strength of water is reduced and thus hydrogen bonding and electrostatic interactions for the guest/host system are enhanced, which was discovered in the research of the molecular recognition of guanidinium/phosphate pairs.[57,58] Although this phenomenon is especially pronounced at air/water interfaces, it is still highly significant also at the water/solid interfaces, which was validated by the same research group through theoretical quantum calculations.[59,60] It should apply to other molecular recognition pairs including but not limited to amino acids, peptides, sugars, nucleic acid bases, and nucleotides as summarized in recent reviews.[61] This enhanced stability shows that the surface immobilization of chemosensors can provide additional advantages over homogeneous solution based sensing assays.

Discussion of Mass Transport Processes. To better understand the differences in surface bound CBn IDA sensing, a deeper look into the mass transport processes is critical: The first mass transport happens between the indicator solution and the CBn microarrays, built on a reversible host−guest interaction[62] where the indicator assembles into CBn mostly driven by uptake kinetics due to the high molecular ratio of indicator to CBn,[63] as shown in surface bound CBn/ indicator.[34] A higher equilibrium constant as mentioned above leads to an enhancement of the mass transport coefficient, which also explains the stability of the CBn/ indicator microarray after the removal of the indicator solution

and exposure to PBS buffer, corresponding again to the homogeneous coating of the CBn/indicator.[35] The second mass transport process to take into account is between the analyte solution and the CBn/indicator microarrays, a reversible indicator replacement process. On one hand, the analyte assembles into CBn by favorable kinetics and higher binding affinity with CBn. On the other hand, the replaced indicator, not being bound anymore in CBn, moves away from the diffusive sublayer just above the surface to the bulk solution entering an entropy increased steady state.[36,62] How much analyte can diffuse to the surface to replace indicators for a given time duration depends on the concentration of the analyte and the volume of the sample solution. In principle, a low concentration and low sample volume can therefore make it necessary to collect all available analyte molecules in a sample (depending on how many sensor molecules are available and needed to react for a detectable signal), thus being mainly limited by the mass transfer to the surface.[64] In our case, it can be seen that full replacement of the available CBn bound indicator on the surface is reached in most cases, so the mass transport suffices for effective sensing, and enough analyte molecules reach the surface to displace all available indicator molecules in equilibrium conditions. However, in the low concentration regimes (e.g., 1 nM of Cad in Figure 4a), analyte molecule diffusion to the surface was too slow to allow full replacement, and only a partial decrease in fluorescence is observed. This shows (as enough analyte molecules will be present in the solution even at low concentration experiments, c.f., the section "Estimation of Analytes to Sensor Molecules Ratio" in the Supporting Information) that in these cases a mass transport limit is reached, when convection and diffusion deliver analytes so slowly to the liquid−solid interface that the time for the reaction itself is negligible by comparison.[65] However, this limitation could be decreased by stirring the system or adding additional fresh analyte solution.

■ CONCLUSIONS

In summary, patterned immobilization of CBn/indicator chemosensors into microarrays was introduced to demonstrate the potential for multiplexed and highly sensitive detection of small molecule analytes. For this, alkyne functionalized CBn were synthesized allowing for covalent linkage on the SiO_2- SH surface to obtain mono/multiplex CBn microarrays through μCS. The resulting CBn microarrays were loaded with indicators, and the thus prepared CBn/indicator microarrays were tested for emissive IDA to detect nonchromophoric analytes. The CBn/indicator microarrays show enhanced detecting sensitivity in the nanomolar range and solve the problem of displaced dye remaining to interfere in the signal readout as it can be simply washed away. Furthermore, the integration of such CBn/indicator microarrays into microfluidic systems provides an efficient method for real time monitoring of the sensing process at the liquid− solid interface, simplifying handling and reducing the need for analyte volume. Finally, the demonstration of multiplex microarrays with multi CBn and/or multi indicator responding differentially to different analytes shows the exquisite potential of surface bound IDA for multicomponent sensing. The demonstrated approach provides significant value for further development of the IDA sensing strategy for multianalyte detection in complex fluids. Furthermore, the multiplexing of CBn enables the building of host−guest sensing libraries,

opening up routes for industrialization in biological or environmental applications.

METHODS

Materials. Details of the materials used can be found in the Supporting Information.

Synthesis of Glycoluril, CB*n*, and CB*n*−OH. Details of the synthesis and structure characterization are provided in the Supporting Information.

Synthesis of Propargyl CB6 (CB6-Pro). First, 50 mg (49.4 μmol, 1 equiv) of CB6 OH was dissolved in 5 mL of 1.2 M potassium iodide (KI) solution/anhydrous DMSO and cooled to 0 °C. Then, 1.46 mL of fresh lithium diisopropylamide (LDA) solution (1.21 mmol, 24.5 equiv) was added under nitrogen, and the mixture was stirred at room temperature for 2 h. Afterward, the mixture was cooled to 0 °C, and 146 μL of propargyl bromide (1.21 mmol, 24.5 equiv, 80% in toluene) was added under nitrogen. Then, the reaction mixture was stirred at room temperature for 24 h. Fifty milliliters of methanol/diethyl ether (V/V = 1:1) solution was added, and the resulting precipitate was triturated with 25 mL of MeOH (3×) and dried at 80 °C for 1 h. The crude product obtained was then reacted again under the same conditions as above to increase the yield (ESI MS: calcd for $[M + C_{16}H_{28}N_4]^{2+}$: 663.2677; found: 663.2572, 22.5%, Figure S24). The analytical data agreed with the literature.[66]

Synthesis of Propargyl CB7 (CB7-Pro). First, 50 mg (42.4 μmol, 1 equiv) of CB7 OH was dissolved in 5 mL of 1.2 M KI solution/anhydrous DMSO and cooled to 0 °C. Then 24.9 mg (1.04 mmol, 24.5 equiv) of NaH (95% purity as solid) was added under nitrogen, and the mixture was stirred at room temperature for 2 h. Afterward, the mixture was cooled to 0 °C again, and 144 μL of propargyl bromide (1.04 mmol, 24.5 equiv, 80% in toluene) was added under nitrogen. Then the reaction mixture was stirred at room temperature for 24 h, and 50 mL of methanol/diethyl ether (V/V = 1:1) solution was added. The resulting precipitate was triturated with 25 mL of MeOH (3×) and dried at 80 °C for 1 h (ESI MS: calcd for $[M + C_{16}H_{28}N_4]^{2+}$ for CB7 $(Pro)_1$: 746.2922, found: 746.2920, 27.8%; calcd for $[M + C_{16}H_{28}N_4]^{2+}$ for CB7 $(Pro)_2$: 773.3021, found: 773.3138, 28.3%; calcd for $[M + C_{16}H_{28}N_4]^{2+}$ for CB7 $(Pro)_3$: 800.3152, found: 800.3022, 23.2%, 79.3% of CB7 Pro in total, Figure S26). The analytical data agreed with the literature.[66]

Synthesis of Propargyl CB8 (CB8-Pro). First, 50 mg (37.2 μmol, 1 equiv) of CB8 OH was dissolved in 5 mL of 1.2 M KI solution/anhydrous DMSO and cooled to 0 °C. Then 1.1 mL of fresh lithium diisopropylamide solution (910 μmol, 24.5 equiv) was added under nitrogen. The mixture was stirred at room temperature for 2 h. Afterward, the mixture was cooled to 0 °C, and 99.8 μL of propargyl bromide (910 μmol, 24.5 equiv, 80% in toluene) was added under nitrogen. Then the reaction mixture was stirred at room temperature for 24 h, and 50 mL of methanol/diethyl ether (V/V = 1:1) solution was added. The resulting precipitate was triturated with 25 mL of MeOH (3×) and dried at 80 °C for 1 h. The crude product obtained was then reacted again under the same conditions to increase the yield (ESI MS: calcd for $[M+C_{16}H_{20}N_4]^{2+}$: 825.2854, found: 825.2831, 22.4%, Figure S30). The analytical data agreed with the literature.[67]

^{1}H NMR. ^{1}H NMR spectra were recorded on a Bruker Avance 500 spectrometer. The ^{1}H NMR chemical shifts (δ) are given in ppm and refer to residual protons on the corresponding deuterated solvent.

ESI-MS. Mass spectroscopy was performed on a micrOTOF Q (208 230 Vac, 50/60 Hz, 1800VA), Bruker. For sample preparation, a trace amount of the samples was dissolved in 1 mL of H_2O/MeOH (V/V = 1:1), and 0.5 mL of 10 mM guest aqueous solution (KCl, $C_{16}H_{28}N_4Br_2$, or $C_{16}H_{20}N_4Br_2$) was added. The samples were treated in an ultrasound bath for several minutes to ensure the host−guest complexes formed.

Surface Modification. A standard glass coverslip SiO_2 (VWR, Germany) was sonicated with chloroform, ethanol, and water for 5 min, respectively. Then, SiO_2 was activated with oxygen plasma (10 sccm O_2, 0.2 mbar, 100 W, 2 min, ATTO system, Diener Electronics, Germany) to get a hydroxylated surface SiO_2−OH. After that, SiO_2−

OH was immersed in 2 vol % MPTMS ((3 mercaptopropyl) trimethoxysilane) in toluene for 5 h. Finally, this substrate was ready to use for lithography after rinsing with acetone for 2 min and water and then dried with N_2. For contact angle and XPS measurements, SiO_2−SH was covered with 5 mg/mL CB7 Pro in DMSO and irradiated under 254 nm UV light for 10 min, and the rest of the solution was washed awqay to get homogeneous SiO_2−CB7.

Ink Preparation. CB6 ink contained 1 mg/mL of crude CB6 Pro in DMSO, 40 vol % 3 mg/mL tris(2 carboxyethyl)phosphine hydrochloride (TCEP) in water, and 20 vol % glycerol. CB7 ink contained 1 mg/mL of CB7 Pro in DMSO, 40 vol % 3 mg/mL of TCEP in water, and 20 vol % glycerol. CB8 ink contained 1 mg/mL of crude CB8 Pro in DMSO, 40 vol % 3 mg/mL of TCEP in water and 20 vol % glycerol. Reference ink included 100 μg/mL of RD in DMSO, 40 vol % 3 mg/mL of TCEP in water, and 20 vol % glycerol. The inks for the printing controls contained 1 mg/mL pure CB7, CB7 OH, or CB7 Pro in DSMO, 40 vol % 3 mg/mL tris(2 carboxyethyl)phosphine hydrochloride (TCEP) in water, and 20 vol % glycerol for each. The solubility of CB7 Pro is lower than that of its crude product used above.

Microchannel Cantilever Spotting (*µ*CS). After modification with thiol groups by silanization, the glass substrate was printed with CB*n* Pro by lithography. A 0.5 μL sample of the prepared ink was applied to the reservoir of the microchannel cantilever[68] (SPT S C10S, Bioforce Nanosciences); the chip was then mounted to the lithography setup (NLP2000, Nanoink), and spotting took place by contacting the tip with the SiO_2−SH surface for defined durations (~0.5−1 s) at a controlled humidity of 40% to prevent premature drying. After printing, the substrate was irradiated under 254 nm UV light for 10 min, then washed with water and ethanol, and finally dried with a nitrogen stream.[69] The rest of the thiols were reacted with N ethylmaleimide acting as a blocking agent through incubation in a 10 mg/mL N ethylmaleimide water solution, pH 7.0, for 2 h.

Contact Angle Measurement. The static contact angles of water droplets on SiO_2 and homogeneously functionalized SiO_2−SH, SiO_2−CB6, SiO_2−CB7, and SiO_2−CB8 were recorded at room temperature through an OCA 20 contact angle analyzer (Data Physics Instruments GmbH). For each measurement, five water droplets with 2 μL were dropped on the surface at the rate of 2 μL s^{-1}, and the average contact angle value was reported.

Characterization by X-ray Photoelectron Spectroscopy (XPS). XPS measurements were performed by a K Alpha+ XPS spectrometer (ThermoFisher Scientific, East Grinstead, U.K.). Data acquisition and processing were obtained by Thermo Avantage software. A microfocused, monochromated Al Kα X ray source (400 μm spot size) was used for sample analysis. The kinetic energy of the electrons was measured using a 180° hemispherical energy analyzer that was operated in the constant analyzer energy mode at 50 eV pass energy for elemental spectra. The K Alpha+ charge compensation system was applied during analysis, with the use of 8 eV energy electrons and low energy argon ions to avoid any localized charge buildup. The spectra were fitted with Voigt profiles (BE uncertainty: ±0.2 eV), and Scofield sensitivity factors were employed for quantification.[70] All spectra were referenced to the C 1s peak (C−C, C−H) at 285.0 eV binding energy controlled using the well known photoelectron peaks of metallic Cu, Ag, and Au, respectively.

Sensor Assembly and Analyte Detection. Dye solutions and analyte solutions were prepared in PBS. For sensor assembly, the CB*n* patterned substrate was covered with 20 μL of dye solution for 1 min, then washed with water, and dried with floated nitrogen. Twenty microliters of analyte solution was later dropped on the substrate. After the corresponding detecting time, it was washed with water and dried with floated nitrogen. Dynamic analyte detection was monitored in a microfluidic channel.

Real-Time Monitoring in Microfluidic Channel. Printed microarrays on matching substrates were mounted with microfluidic channels (sticky Slide VI 0.4 Luer, ibidi Germany) and set on the microscope. In each of the six channels, solutions with indicators or analytes and buffer were added always from one on chip reservoir (the Luer connector) and removed from the channel's other side reservoir

by manually pipetting 100 μL each time (the chips can accommodate 30 μL in the channel, plus 60 μL in each reservoir). Before analyte detection, chips were washed in this way by buffer until excess indicator was removed from the channel and arrays were clearly visible in the microscope. Then, the buffer was pipetted off, and an analyte solution of the desired concentration was introduced by pipetting on 100 μL again (3× for Spm within a minute, 1× for Cad detection, as here the detection process is happening on a much shorter time scale). The whole process was monitored and recorded to videos by microscope.

Fluorescence Microscopy. The fluorescence imaging was performed on a Nikon Eclipse Ti2 inverted fluorescence microscope (Nikon, Germany) equipped with an Intensilight illumination, a Nikon DS Qi2 camera, and DIA, Cy3, GFP, and DAPI filters sets (Nikon Y 2E/C).

Statistical Analysis. All data were expressed as the means plus/minus standard deviations of more than three independent measurements. The experimentally significant differences were evaluated using analysis of variance (ANOVA). The statistical significance was defined as $p < 0.05$.

ASSOCIATED CONTENT

● **Supporting Information**

The Supporting Information is available free of charge at https://pubs.acs.org/doi/10.1021/acsanm.1c00293.

Additional figures and schemes (PDF)
Scheme of μCS (MP4)
Cad detection (MP4)
Spm detection vs control (MP4)
Scheme of multiplexed detection (MP4)

AUTHOR INFORMATION

Corresponding Authors

Frank Biedermann − *Institute of Nanotechnology (INT), Karlsruhe Institute of Technology (KIT), 76344 Eggenstein Leopoldshafen, Germany;* ● orcid.org/0000 0002 1077 6529; Email: frank.biedermann@kit.edu

Michael Hirtz − *Institute of Nanotechnology (INT) and Karlsruhe Nano Micro Facility (KNMF), Karlsruhe Institute of Technology (KIT), 76344 Eggenstein Leopoldshafen, Germany;* ● orcid.org/0000 0002 2647 5317; Email: michael.hirtz@kit.edu

Authors

Chunting Zhong − *Institute of Nanotechnology (INT) and Karlsruhe Nano Micro Facility (KNMF), Karlsruhe Institute of Technology (KIT), 76344 Eggenstein Leopoldshafen, Germany*

Changming Hu − *Institute of Nanotechnology (INT), Karlsruhe Institute of Technology (KIT), 76344 Eggenstein Leopoldshafen, Germany*

Ravi Kumar − *Institute of Nanotechnology (INT) and Karlsruhe Nano Micro Facility (KNMF), Karlsruhe Institute of Technology (KIT), 76344 Eggenstein Leopoldshafen, Germany*

Vanessa Trouillet − *Institute of Applied Materials (IAM) and Karlsruhe Nano Micro Facility (KNMF), Karlsruhe Institute of Technology (KIT), 76344 Eggenstein Leopoldshafen, Germany*

Complete contact information is available at:
https://pubs.acs.org/10.1021/acsanm.1c00293

Notes
The authors declare no competing financial interest.

REFERENCES

(1) Meldal, M.; Schoffelen, S. Recent Advances in Covalent, Site Specific Protein Immobilization. *F1000Research* **2016**, *5* (0), 2303.

(2) Sassolas, A.; Leca Bouvier, B. D.; Blum, L. J. L. J. DNA Biosensors and Microarrays. *Chem. Rev.* **2008**, *108* (1), 109−139.

(3) Neagu, M.; Bostan, M.; Constantin, C. Protein Microarray Technology: Assisting Personalized Medicine in Oncology (Review). *World Acad. Sci. J.* **2019**, 113−124.

(4) Guerrini, L.; Alvarez Puebla, R. A. Multiplex SERS Chemo sensing of Metal Ions via DNA Mediated Recognition. *Anal. Chem.* **2019**, *91* (18), 11778−11784.

(5) Zhang, S.; Ding, J.; Liu, Y.; Kong, J.; Hofstetter, O. Development of a Highly Enantioselective Capacitive Immunosensor for the Detection of α Amino Acids. *Anal. Chem.* **2006**, *78* (21), 7592−7596.

(6) Dabrowski, M.; Lach, P.; Cieplak, M.; Kutner, W. Nano structured Molecularly Imprinted Polymers for Protein Chemo sensing. *Biosens. Bioelectron.* **2018**, *102*, 17−26.

(7) Wasserberg, D.; Jonkheijm, P. Supramolecular Wearable Sensors. *Chem.* **2017**, *3* (4), 531−533.

(8) Sasaki, Y.; Kubota, R.; Minami, T. Molecular Self Assembled Chemosensors and Their Arrays. *Coord. Chem. Rev.* **2021**, *429*, 213607.

(9) Klimek Tulwin, M.; Knap, J.; Reda, M.; Masternak, M. History of Glucose Monitoring: Past, Present, Future. *J. Educ. Heal. Sport* **2019**, *9* (9), 222−227.

(10) Orooji, Y.; Sohrabi, H.; Hemmat, N.; Oroojalian, F.; Baradaran, B.; Mokhtarzadeh, A.; Mohaghegh, M.; Karimi Maleh, H. An Overview on SARS CoV 2 (COVID 19) and Other Human Coronaviruses and Their Detection Capability via Amplification Assay, Chemical Sensing, Biosensing, Immunosensing, and Clinical Assays. *Nano Micro Lett.* **2021**, *13* (1), 18.

(11) Atwater, J.; Mattes, D. S.; Streit, B.; von Bojničić Kninski, C.; Loeffler, F. F.; Breitling, F.; Fuchs, H.; Hirtz, M. Combinatorial Synthesis of Macromolecular Arrays by Microchannel Cantilever Spotting (MCS). *Adv. Mater.* **2018**, *30* (31), 1801632.

(12) Das, S.; Kumar, R.; Parbat, D.; Sekula Neuner, S.; Hirtz, M.; Manna, U. Covalently Modulated and Transiently Visible Writing: Rational Association of Two Extremes of Water Wettabilities. *ACS Appl. Mater. Interfaces* **2020**, *12* (2), 2935−2943.

(13) Arrabito, G.; Ferrara, V.; Ottaviani, A.; Cavaleri, F.; Cubisino, S.; Cancemi, P.; Ho, Y. P.; Knudsen, B. R.; Hede, M. S.; Pellerito, C.; Desideri, A.; Feo, S.; Pignataro, B. Imbibition of Femtoliter Scale DNA Rich Aqueous Droplets into Porous Nylon Substrates by Molecular Printing. *Langmuir* **2019**, *35* (52), 17156−17165.

(14) Wu, D.; Sedgwick, A. C.; Gunnlaugsson, T.; Akkaya, E. U.; Yoon, J.; James, T. D. Fluorescent Chemosensors: The Past, Present and Future. *Chem. Soc. Rev.* **2017**, *46* (23), 7105−7123.

(15) Chan, J.; Dodani, S. C.; Chang, C. J. Reaction Based Small Molecule Fluorescent Probes for Chemoselective Bioimaging. *Nat. Chem.* **2012**, *4* (12), 973−984.

(16) Chen, X.; Zhou, Y.; Peng, X.; Yoon, J. Fluorescent and Colorimetric Probes for Detection of Thiols. *Chem. Soc. Rev.* **2010**, *39* (6), 2120.

(17) Bell, T. W.; Hext, N. M. Supramolecular Optical Chemosensors for Organic Analytes. *Chem. Soc. Rev.* **2004**, *33* (9), 589−598.

(18) Ramakrishnam Raju, M. V.; Harris, S. M.; Pierre, V. C. Design and Applications of Metal Based Molecular Receptors and Probes for Inorganic Phosphate. *Chem. Soc. Rev.* **2020**, *49* (4), 1090−1108.

(19) Prabodh, A.; Bauer, D.; Kubik, S.; Rebmann, P.; Klärner, F. G.; Schrader, T.; Delarue Bizzini, L.; Mayor, M.; Biedermann, F. Chirality Sensing of Terpenes, Steroids, Amino Acids, Peptides and Drugs with Acyclic Cucurbit[n]Urils and Molecular Tweezers. *Chem. Commun.* **2020**, *56* (34), 4652−4655.

(20) Pinalli, R.; Pedrini, A.; Dalcanale, E. Biochemical Sensing with Macrocyclic Receptors. *Chem. Soc. Rev.* **2018**, *47* (18), 7006−7026.

(21) Sinn, S.; Biedermann, F. Chemical Sensors Based on Cucurbit[n]Uril Macrocycles. *Isr. J. Chem.* **2018**, *58* (3−4), 357−412.

(22) Prabodh, A.; Sinn, S.; Grimm, L.; Miskolczy, Z.; Megyesi, M.; Biczók, L.; Bräse, S.; Biedermann, F. Teaching Indicators to Unravel the Kinetic Features of Host Guest Inclusion Complexes. *Chem. Commun.* **2020**, *56* (82), 12327−12330.

(23) Barba Bon, A.; Pan, Y.; Biedermann, F.; Guo, D.; Nau, W. M.; Hennig, A. Fluorescence Monitoring of Peptide Transport Pathways into Large and Giant Vesicles by Supramolecualar Host Dye Reporter Pairs. *J. Am. Chem. Soc.* **2019**, *141* (51), 20137−20145.

(24) Sinn, S.; Spuling, E.; Bräse, S.; Biedermann, F. Rational Design and Implementation of a Cucurbit[8]Uril Based Indicator Displace ment Assay for Application in Blood Serum. *Chem. Sci.* **2019**, *10* (27), 6584−6593.

(25) Salmon, A. R.; Esteban, R.; Taylor, R. W.; Hugall, J. T.; Smith, C. A.; Whyte, G.; Scherman, O. A.; Aizpurua, J.; Abell, C.; Baumberg, J. J. Monitoring Early Stage Nanoparticle Assembly in Microdroplets by Optical Spectroscopy and SERS. *Small* **2016**, *12* (13), 1788−1796.

(26) Sigle, D. O.; Kasera, S.; Herrmann, L. O.; Palma, A.; de Nijs, B.; Benz, F.; Mahajan, S.; Baumberg, J. J.; Scherman, O. A. Observing Single Molecules Complexing with Cucurbit[7]Uril through Nanogap Surface Enhanced Raman Spectroscopy. *J. Phys. Chem. Lett.* **2016**, *7* (4), 704−710.

(27) Ghale, G.; Nau, W. M. Dynamically Analyte Responsive Macrocyclic Host Fluorophore Systems. *Acc. Chem. Res.* **2014**, *47* (7), 2150−2159.

(28) Sedgwick, A. C.; Brewster, J. T.; Wu, T.; Feng, X.; Bull, S. D.; Qian, X.; Sessler, J. L.; James, T. D.; Anslyn, E. V.; Sun, X. Indicator Displacement Assays (IDAs): The Past, Present and Future. *Chem. Soc. Rev.* **2021**, *50* (1), 9−38.

(29) Nguyen, B. T.; Anslyn, E. V. Indicator Displacement Assays. *Coord. Chem. Rev.* **2006**, *250* (23−24), 3118−3127.

(30) Hu, C.; Grimm, L.; Prabodh, A.; Baksi, A.; Siennicka, A.; Levkin, P. A.; Kappes, M. M.; Biedermann, F. Covalent Cucurbit[7] Uril Dye Conjugates for Sensing in Aqueous Saline Media and Biofluids. *Chem. Sci.* **2020**, *11* (41), 11142−11153.

(31) Wiemann, M.; Jonkheijm, P. Stimuli Responsive Cucurbit[n] Uril Mediated Host Guest Complexes on Surfaces. *Isr. J. Chem.* **2018**, *58* (3−4), 314−325.

(32) Brinkmann, J.; Wasserberg, D.; Jonkheijm, P. Redox Active Host Guest Supramolecular Assemblies of Peptides and Proteins at Surfaces. *Eur. Polym. J.* **2016**, *83*, 380−389.

(33) Hwang, I.; Baek, K.; Jung, M.; Kim, Y.; Park, K. M.; Lee, D. W.; Selvapalam, N.; Kim, K. Noncovalent Immobilization of Proteins on a Solid Surface by Cucurbit[7]Uril Ferrocenemethylammonium Pair, a Potential Replacement of Biotin Avidin Pair. *J. Am. Chem. Soc.* **2007**, *129* (14), 4170−4171.

(34) Jon, S. Y.; Selvapalam, N.; Oh, D. H.; Kang, J. K.; Kim, S. Y.; Jeon, Y. J.; Lee, J. W.; Kim, K. Facile Synthesis of Cucurbit[n]Uril Derivatives via Direct Functionalization: Expanding Utilization of Cucurbit[n]Uril. *J. Am. Chem. Soc.* **2003**, *125* (34), 10186−10187.

(35) Zhang, F.; Lu, C.; Wang, M.; Yu, X.; Wei, W.; Xia, Z. A Chiral Sensor Array for Peptidoglycan Biosynthesis Monitoring Based on MoS2 Nanosheet Supported Host Guest Recognitions. *ACS Sensors* **2018**, *3* (2), 304−312.

(36) Zhu, X.; Fan, X.; Ju, G.; Cheng, M.; An, Q.; Nie, J.; Shi, F. A Facile Method to Immobilize Cucurbituril on Surfaces through Photocrosslinking with Azido Groups. *Chem. Commun.* **2013**, *49* (73), 8093−8095.

(37) Lee, D. W.; Park, K. M.; Gong, B.; Shetty, D.; Khedkar, J. K.; Baek, K.; Kim, J.; Ryu, S. H.; Kim, K. A Simple Modular Aptasensor Platform Utilizing Cucurbit[7]Uril and a Ferrocene Derivative as an Ultrastable Supramolecular Linker. *Chem. Commun.* **2015**, *51* (15), 3098−3101.

(38) Gomez Casado, A.; Jonkheijm, P.; Huskens, J. Recognition Properties of Cucurbit[7]Uril Self Assembled Monolayers Studied with Force Spectroscopy. *Langmuir* **2011**, *27* (18), 11508−11513.

(39) An, Q.; Brinkmann, J.; Huskens, J.; Krabbenborg, S.; de Boer, J.; Jonkheijm, P. A Supramolecular System for the Electrochemically Controlled Release of Cells. *Angew. Chem., Int. Ed.* **2012**, *51* (49), 12233−12237.

(40) González Campo, A.; Brasch, M.; Uhlenheuer, D. A.; Gómez Casado, A.; Yang, L.; Brunsveld, L.; Huskens, J.; Jonkheijm, P. Supramolecularly Oriented Immobilization of Proteins Using Cucurbit[8]Uril. *Langmuir* **2012**, *28* (47), 16364−16371.

(41) Tian, F.; Jiao, D.; Biedermann, F.; Scherman, O. A. Orthogonal Switching of a Single Supramolecular Complex. *Nat. Commun.* **2012**, *3* (1), 1207.

(42) Tian, F.; Cziferszky, M.; Jiao, D.; Wahlström, K.; Geng, J.; Scherman, O. A. Peptide Separation through a CB[8] Mediated Supramolecular Trap and Release Process. *Langmuir* **2011**, *27* (4), 1387−1390.

(43) Nair, R. R.; Debnath, S.; Das, S.; Wakchaure, P.; Ganguly, B.; Chatterjee, P. B. A Highly Selective Turn On Biosensor for Measuring Spermine/Spermidine in Human Urine and Blood. *ACS Appl. Bio Mater.* **2019**, *2* (6), 2374−2387.

(44) Fletcher, J. T.; Bruck, B. S. Spermine Detection via Metal Mediated Ethynylarene 'Turn on' Fluorescence Signaling. *Sens. Actuators, B* **2015**, *207*, 843−848.

(45) Kaur, N.; Chopra, S.; Singh, G.; Raj, P.; Bhasin, A.; Sahoo, S. K.; Kuwar, A.; Singh, N. Chemosensors for Biogenic Amines and Biothiols. *J. Mater. Chem. B* **2018**, *6* (30), 4872−4902.

(46) Thomas, A.; Iacono, D.; Luciano, A. L.; Armellino, K.; Di Iorio, A.; Onofrj, M. Duration of Amantadine Benefit on Dyskinesia of Severe Parkinson's Disease. *J. Neurol. Neurosurg. Psychiatry* **2004**, *75* (1), 141−143.

(47) Dadfar, S. M. M.; Sekula Neuner, S.; Trouillet, V.; Hirtz, M. A Comparative Study of Thiol Terminated Surface Modification by Click Reactions: Thiol Yne Coupling versus Thiol Ene Michael Addition. *Adv. Mater. Interfaces* **2018**, *5* (24), 1801343.

(48) Lagona, J.; Mukhopadhyay, P.; Chakrabarti, S.; Isaacs, L. The Cucurbit[n]Uril Family. *Angew. Chem., Int. Ed.* **2005**, *44* (31), 4844− 4870.

(49) Lowe, A. B.; Hoyle, C. E.; Bowman, C. N. Thiol Yne Click Chemistry: A Powerful and Versatile Methodology for Materials Synthesis. *J. Mater. Chem.* **2010**, *20* (23), 4745−4750.

(50) Rekharsky, M. V.; Ko, Y. H.; Selvapalam, N.; Kim, K.; Inoue, Y. Complexation Thermodynamics of Cucurbit[6]Uril with Aliphatic Alcohols, Amines, and Diamines. *Supramol. Chem.* **2007**, *19* (1−2), 39−46.

(51) Sindelar, V.; Cejas, M. A.; Raymo, F. M.; Kaifer, A. E. Tight Inclusion Complexation of 2,7 Dimethyldiazapyrenium in Cucurbit[7]Uril. *New J. Chem.* **2005**, *29* (2), 280.

(52) Miskolczy, Z.; Megyesi, M.; Biczók, L.; Prabodh, A.; Biedermann, F. Kinetics and Mechanism of Cation Induced Guest Release from Cucurbit[7]Uril. *Chem. Eur. J.* **2020**, *26* (33), 7433− 7441.

(53) Bailey, D. M.; Hennig, A.; Uzunova, V. D.; Nau, W. M. Supramolecular Tandem Enzyme Assays for Multiparameter Sensor Arrays and Enantiomeric Excess Determination of Amino Acids. *Chem. Eur. J.* **2008**, *14* (20), 6069−6077.

(54) Sinn, S.; Krämer, J.; Biedermann, F. Teaching Old Indicators Even More Tricks: Binding Affinity Measurements with the Guest Displacement Assay (GDA). *Chem. Commun.* **2020**, *56* (49), 6620− 6623.

(55) Das, D.; Assaf, K. I.; Nau, W. M. Applications of Cucurbiturils in Medicinal Chemistry and Chemical Biology. *Front. Chem.* **2019**, *7*, 619.

(56) Wenz, G.; Weickenmeier, M.; Huff, J. Association Thickener by Host—Guest Interaction of β Cyclodextrin Polymers and Guest Polymers. *ACS Symp. Ser.* **2000**, *765*, 271−283.

(57) Onda, M.; Yoshihara, K.; Koyano, H.; Ariga, K.; Kunitake, T. Molecular Recognition of Nucleotides by the Guanidinium Unit at the Surface of Aqueous Micelles and Bilayers. A Comparison of Microscopic and Macroscopic Interfaces. *J. Am. Chem. Soc.* **1996**, *118* (36), 8524−8530.

(58) Cha, X.; Ariga, K.; Onda, M.; Kunitake, T. Molecular Recognition of Aqueous Dipeptides by Noncovalently Aligned Oligoglycine Units at the Air/Water Interface. *J. Am. Chem. Soc.* **1995**, *117* (48), 11833−11838.

(59) Sakurai, M.; Tamagawa, H.; Inoue, Y.; Ariga, K.; Kunitake, T. Theoretical Study of Intermolecular Interaction at the Lipid Water Interface. 1. Quantum Chemical Analysis Using a Reaction Field Theory. *J. Phys. Chem. B* **1997**, *101* (24), 4810−4816.

(60) Tamagawa, H.; Sakurai, M.; Inoue, Y.; Ariga, K.; Kunitake, T. Theoretical Study of Intermolecular Interaction at the Lipid Water Interface. 2. Analysis Based on the Poisson Boltzmann Equation. *J. Phys. Chem. B* **1997**, *101* (24), 4817−4825.

(61) Ariga, K.; Makita, T.; Ito, M.; Mori, T.; Watanabe, S.; Takeya, J. Review of Advanced Sensor Devices Employing Nanoarchitectonics Concepts. *Beilstein J. Nanotechnol.* **2019**, *10*, 2014−2030.

(62) Versteeg, G. F.; Kuipers, J. A. M.; Van Beckum, F. P. H.; Van Swaaij, W. P. M. Mass Transfer with Complex Reversible Chemical Reactions—I. Single Reversible Chemical Reaction. *Chem. Eng. Sci.* **1989**, *44* (10), 2295−2310.

(63) Jangara, H.; Shayesteh, K.; Shahedi Asl, M. Mathematical Modeling of Absorption Accompanied by a Non Elementary Reversible Chemical Reaction. *Chem. Eng. Res. Des.* **2020**, *157*, 58−64.

(64) Squires, T. M.; Messinger, R. J.; Manalis, S. R. Making It Stick: Convection, Reaction and Diffusion in Surface Based Biosensors. *Nat. Biotechnol.* **2008**, *26* (4), 417−426.

(65) Sanford, L. P.; Crawford, S. M. Mass Transfer versus Kinetic Control of Uptake across Solid Water Boundaries. *Limnol. Oceanogr.* **2000**, *45* (5), 1180−1186.

(66) Zhang, S.; Domínguez, Z.; Assaf, K. I.; Nilam, M.; Thiele, T.; Pischel, U.; Schedler, U.; Nau, W. M.; Hennig, A. Precise Supramolecular Control of Surface Coverage Densities on Polymer Micro and Nanoparticles. *Chem. Sci.* **2018**, *9* (45), 8575−8581.

(67) Kim, K.; Selvapalam, N.; Ko, Y. H.; Park, K. M.; Kim, D.; Kim, J. Functionalized Cucurbiturils and Their Applications. *Chem. Soc. Rev.* **2007**, *36* (2), 267−279.

(68) Xu, J.; Lynch, M.; Huff, J. L.; Mosher, C.; Vengasandra, S.; Ding, G.; Henderson, E. Microfabricated Quill Type Surface Patterning Tools for the Creation of Biological Micro/Nano Arrays. *Biomed. Microdevices* **2004**, *6* (2), 117−123.

(69) Nagarajan, E. R.; Oh, D. H.; Selvapalam, N.; Ko, Y. H.; Park, K. M.; Kim, K. Cucurbituril Anchored Silica Gel. *Tetrahedron Lett.* **2006**, *47* (13), 2073−2075.

(70) Scofield, J. H. Hartree Slater Subshell Photoionization Cross Sections at 1254 and 1487 EV. *J. Electron Spectrosc. Relat. Phenom.* **1976**, *8* (2), 129−137.